Chapter 6

Bio-Inspired Photonic Structures: Prototypes, Fabrications and Devices

Feng Liu, Biqin Dong and Xiaohan Liu

Additional information is available at the end of the chapter

http://dx.doi.org/10.5772/50199

1. Introduction

Like the ability of electron regulation of electronic semiconductors, the photonic analogs usually considered as photonic structure materials are regarded as essential for light manipulation [1, 2]. With particular designs of photonic structures, they are expected to achieve different far-field and near-field optical features and thus lead to a perspective in all-optical circuit [3]. Though humankind has entered the nano-scale realm several decades ago, it is still a hard task for engineers to explore novel optical functional devices due to the limited experiences and originalities on artificial photonic structures design and the desired optical features. Additionally, it is also great challenges to fabricate photonic structures, owing to their sub-optical-wavelength to sub-micron featured sizes, especially in a high dimensional way by nano-fabrication technologies today.

By contrast, nature are found to develop photonic structures millions of years before our initial attempts. Diversified photonic structures, most of which are sophisticated and hierarchic, are revealed in beetles, butterflies, sea animals and even plants in recent surveys [4–10]. The exhibited optical features are regarded to have particular biological functions such as signal communications, conspecific recognition, and camouflage, which are optimized under selection pressure. Naturally, the occurring photonic structures provide us ideal 'blueprints' on design and stimulate similar optical functional devices. Various fabrication methods of bio-inspired photonic structures are explored [11–16]. By chemical methods (e.g. Sol-Gel, colloidal crystallization, chemical systhesis), nanoimprint lithography and nanocasting, physical layer deposition (PLD), atomic layer deposition (ALD), and etc., bio-inspired photonic structures, their reverse counterparts, and applications are achieving greater success than ever before.

This Chapter will review the typical bio-inspired photonic structures and focus on the biomimetic fabrications, the corresponding optical functions and the prototypes of optical devices. It is organized as follows: four subsections are introduced in Section 2, in which each describes one catagory of bio-inspired optical functional devices. In every subsection, the nature prototype is introduced first, then followed by biomimetic fabrication methods and

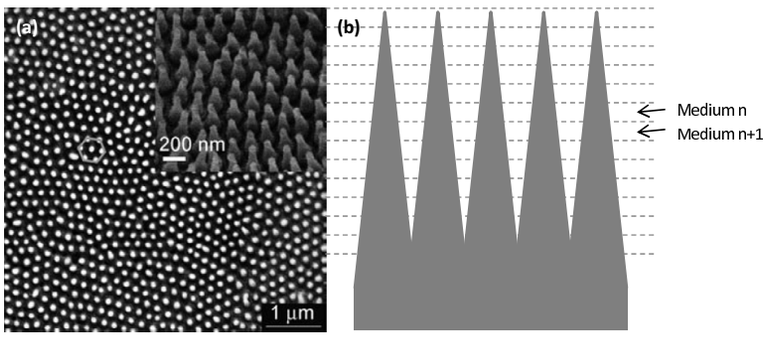

Figure 1. Antireflection structures. (a) Hexagonal arranged tapered pillars root in the surface of cicada wings in top view (tilted view of the pillar array is showed in the inset) [19]; (b) The tapered pillars lead to gradual refraction index variation in view of effective theory and then minimize the reflection according to Fresnel relations.

optical features of artificial analogs, finally closed on the bio-inspired optical devices. A brief perspective is given in Section 3.

2. Bio-inspired optical functional devices

2.1. Anti-reflection devices

2.1.1. Prototypes

In arthropodal animals such as butterflies, nipple arrays with typical spacing of optical wavelength or subwavelength are commonly found on surfaces of their compound eyes, which are believed helpful to the light-harvest efficiency of the biological visual system [17]. With optical impedance matching to the ambience, the light transmission are enhanced. Another analogous examples are the transparent wings of some lepidoptera insects like hawkmoths [18] and cicada [19] (Fig.1 (a)). The tapered pillars lead to gradual changes of refraction index in view of effective medium theory (Fig.1 (b)) and therefore play a key role in minimizing the reflection over broadband and large viewangles. In order to physically explain the anti-reflection origin, the Fresnel equations are given as follows.

$$r_s = |\frac{n_1 cosi_1 - n_2 cosi_2}{n_1 cosi_1 + n_2 cosi_2}|, \tag{1}$$

$$r_p = |\frac{n_1 cosi_2 - n_2 cosi_1)}{(n_1 cosi_2 + n_2 cosi_1}|, \tag{2}$$

where r_s and r_p refer to reflection coefficients of s polarised light (the electric field of the light perpendicular to the incident plane) and p polarised light (the electric field in the incident light plane), n_1 and n_2 are refraction indices of neighboring mediums, respectively. The relationship between incident angle i_1 and refraction angle i_2 is given by Snell's Law $n_1 \sin i_1 = n_2 \sin i_2$. From the equations, e.g., for normal incidence, r_s and r_p are suppressed to near zero if n_1 and n_2 have very close values [20, 21].

2.1.2. Bio-inspired fabrications

Inspired by nature, many efforts are made in exploring techniques for fabricating the anti-reflection nanostructures and a variety of methods, e.g., conformal-

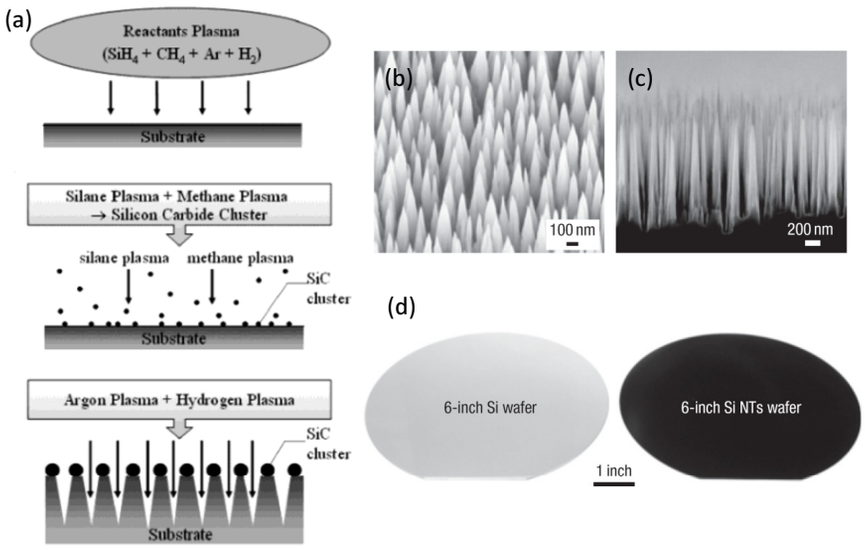

Figure 2. Improved antireflection of biomimetic nanotips by ECR plasma etching technique [25, 27]. (a) Schematic diagram for the silicon nanotip formation on silicon wafer; (b) and (c) show a tilted top view and a cross-sectional view of silicon nanotips, respectively; (d) Compared with polished silicon wafer (left), 6-inch silicon wafer coated with silicon nanotips (right) show greatly improved broadband and quasi omnidirectional anti-reflection.

evaporated-film-by-rotation (CEFR), colloidal lithography, self-masked dry etching, nanoimprint lithography (NIL), ALD and other approaches, are realized [16].

Oblique angle deposition (OAD) is usually employed to fabricate anisotropic film which is originated from the oblique growth of contained nanorods with a tilted angle to the substrate surface normal. The so-called CEFR method, which rotates the substrates at a high speed under OAD, leads to the straight growth of a dense array columns to substrate surface rather than helical structures which are formed under low rotation rate. That is, CEFR method is suitable for conformal replication of the photonic structure with a curved surface even under thick film deposition. With compound eyes of the fruit fly as bio-templates, it is reported artificial replica is successfully fabricated and hence similar optical features are inherited, respectively [22].

Many lithography techniques are applied for fabricating antireflection structures, among which colloidal lithography is a much simpler approach [23]. With colloidal crystals as masks, the silicon substrate is etched by reaction ion etching (RIE). During the fabrication duration, the colloidal spheres are etched by RIE gradually firstly, leading to a reduced transverse cross section of the spheres and thus an increasing exposure of the substrate. Attributed to the features of RIE, the etching rates of the apex and the junction parts of the spheres are not uniform, resulting in the etching morphology modification from frustum to cone arrays on the substrate finally [24].

Electron cyclotron resonance (ECR) plasma etching technique is employed by researchers to fabricate antireflection structures with much higher aspect ratio surfaces [25–27]. With the selected gas-mixture consisting of SiH_4, CH_4, Ar, and H_2, one step and self-masked dry etching are realized for fabricating high density nanotip arrays on a 6-inch silicon wafer. The fabrication progress is illustrated in the schematic diagram of Fig. 2(a). In brief, SiC clusters, which size and density can be tuned via process temperature, gas pressure, and composition, are formed on surfaces of the silicon substrate due to the reaction of SiH_4 and CH_4 plasma.

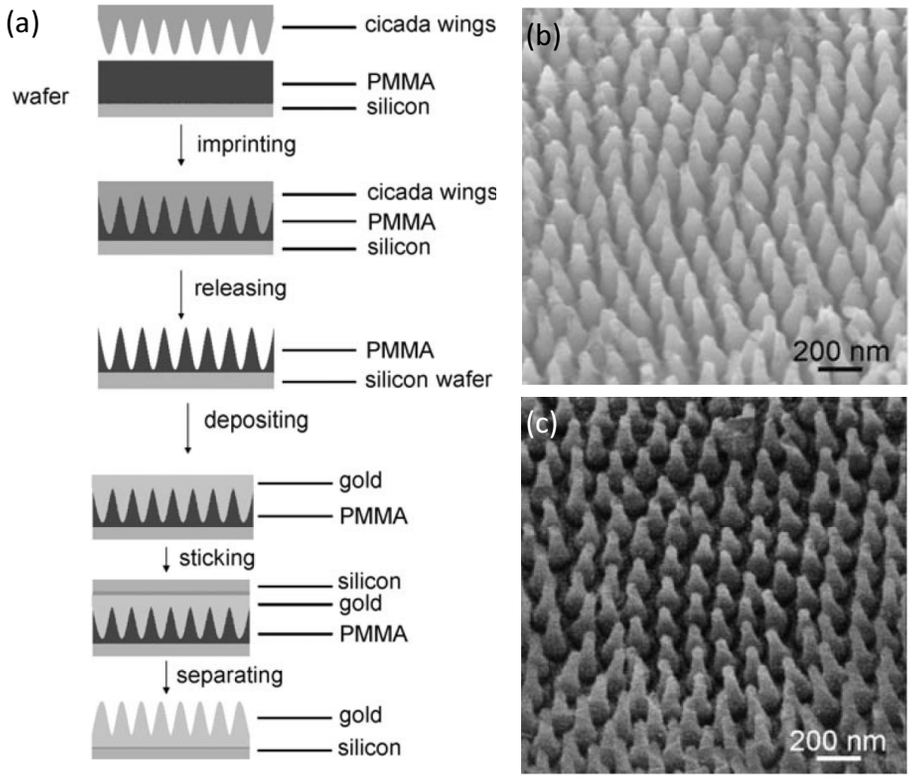

Figure 3. Cicada wing structure fabrication by NIL [19]. (a) Schematic diagram of NIL using cicada wings as bio-templates; (b) The fabricated structures and (c) the natural photonic structures show similar morphology from the SEM images.

Ar and H_2 are responsible for the dry etching process. The SiC clusters then act as nanomasks or nanocaps to protect the underlying substrate from etching, thus forming an aperiodic array of silicon nanotips with their lengths varying from $\sim$1000 nm to $\sim$ 16 μm finally (Fig. 2(b) and (c)). Even superior to natural prototypes, the biomimetic antireflection structures exhibit striking omnidirectional low reflection shown in Fig. 2(d) over a broad range of wavelengths from ultraviolet to terahertz region, irrespective of polarization.

Avoiding time-consuming and complicated mask fabrication, scientists also attempt to directly use cicada wings or insect eyes as bio-templates [19, 28, 29]. For example, the nipple arrays on wing surfaces are stamped under certain pressure on glass-phase PMMA, which is at higher degree than its glass-transition temperature, supported by silicon wafer. A release process makes the polymer reverse nanostructures of the bio-templates. With the patterned PMMA as a mask or a mold, inverse or similar structures of the cicada wing are achieved by RIE or thermodeposition. A schematic diagram of the NIL, the fabricated structures, and the natural templates for comparison are illustrated in Fig. 3(a), Fig. 3(b), and Fig. 3(c), respectively. It is also worthy to note that an extra advantage of using bio-templates in NIL process is the notable low-surface-tension, which is vital for the release process, due to the wax layer commonly found on surfaces of plants and insects.

Taking advantages of accurate thickness control and three-dimensional (3D) fabrication of ALD, conformal replica is accomplished after ALD growth and sintering the hybrid structures with fly eyes as bio-templates, achieving similar anti-reflective features in the artificial analog finally [29].

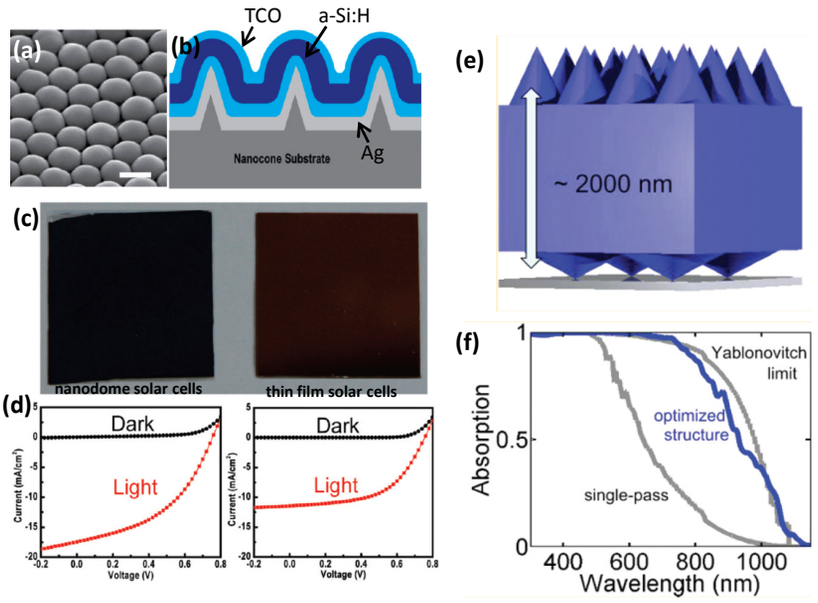

Figure 4. (Color online) Solar cells coating antireflection structures [32, 34]. (a) Nanodome solar cells in top view. Scale bar 500 nm; (b) Schematic diagram of the cross-sectional structures of the solar cells; (c) The photographs of nanodome solar cells (left) and flat film solar cells (right); (d) Dark and light I-V curve corresponding to (c); (e) and (f) The optimized double-sided nanostructure yields a photocurrent close to the Yablonovitch limit at an equivalent thickness of 2 μm.

2.1.3. Potential applications

Due to the high reflectance of silicon solar cells (more than 30%) induced by the high index contrast of silicon and air according to the Fresnel equations, scientists are already aware of the vital roles of high-quality antireflection coatings at early ages of solar cell fabrications [30]. Inspired by antireflection structures found in moth eyes, nanodomes or similar architectures are reproduced on surfaces of solar cells, leading to a dramatic light absorption increase and therefore a superior efficiency improvements than that of quarter-wavelength antireflection coating [31–33], as shown in Fig. 4(a)-(d). The recent theoretical investigations even report a high light trapping close to the Yablonovitch limit in the silicon solar cell by optimizing a double-sided antireflection structure design (Fig. 4(e) and (f))[34].

The biomimetic antireflection structures can also play a key role in light extraction of light-emitting devices (LEDs) [35–37]. Because of the total internal reflection and the waveguiding modes in the glass substrate, only about 20% amount of the generated light can irradiate from the LEDs. By fabricating silica cone arrays on the surfaces of the ITO glass substrate to modulate the above two bottleneck factors, the light luminance efficiency of white LEDs is significantly improved by a factor of 1.4 in the normal direction and even larger enhancement for large viewing angles.

Another fascinating application of the inspired antireflection structures is the use in the micro Sun sensor for Mars rovers [38]. On the basis of the recorded image by an active pixel sensor, the location coordinates of the rover can be calculated. However, the ghost image originating from the multiple internal reflection of the optical system leads to severe limitation of the accuracy. By fabricating dense nanotip arrays on the surfaces of the sensor, the internal reflection is minimized to be nearly 3 orders of magnitude lower than that of no treatments, resulting in a more reliable three-axis attitude information.

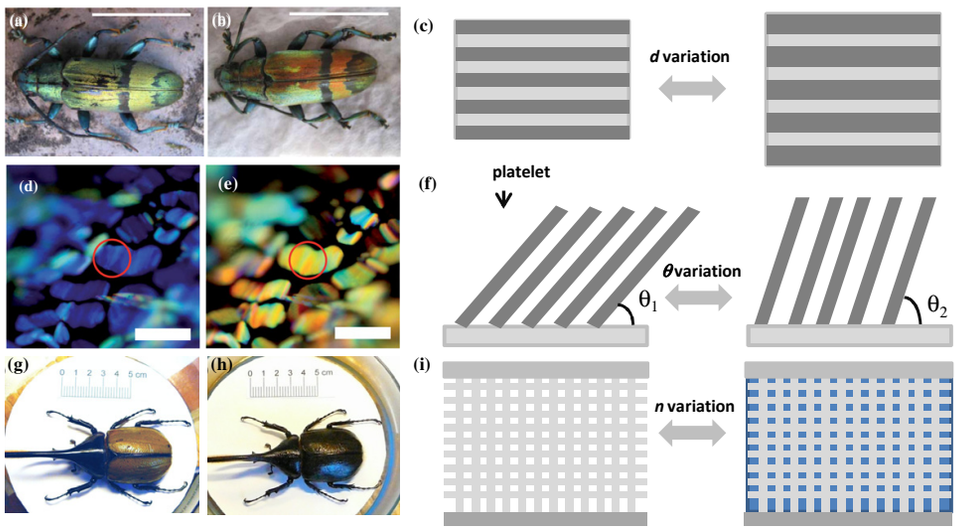

Figure 5. (Color online) Color tuning mechanisms found in nature [50, 53, 56]. The coloration of (a) longhorn beetles, (d) iridophore of tropic fish neon tetra, and (g) hercules beetles can reversibly change their coloration to (b), (e), and (h), which are intrinsically induced by (c) period d, (f) tilting angle θ, (i) refraction index n variation, respectively. Scale bars: (a) and (b) 10 mm, (d) and (e) 20 μm.

2.2. Color-tunable devices

2.2.1. Prototypes

Besides the well known coloration change strategy via migrations and volumes change of pigment granules such as chameleons, nature develops a second approach which is known as structural coloration change (SCC). By varying photonic structure characterizations, incident light angle, or the refraction index contrast of the color-produced optical system via the environmental stimuli, reversible coloration changes, which are basically passive, are revealed in fishes, beetles, and birds [39–46]. Most structural basis of SCC are attributed to the one-dimensional (1D) reflectors. For example, the damselfish *Chrysiptera cyanea* can change its color from blue to ultraviolet rapidly under stressful conditions, which is triggered by the simultaneous change in the spacing of adjoining reflecting plates made of guanine in the iridophore cell [47–49]. In insect world, the coloration change of longhorn beetles *Tmesisternus isabellae* from golden to red is revealed to originate from the swollen multilayer after water absorption [50] (Fig. 5(a), (b) and (c)). Another origin of structural coloration change is the tilted angle variability of the nanoplates with respect to incident light, which is found in tropic fish neon tetra *Paracheirodon innesi* [51–53] (Fig. 5(d), (e), and (f)). Physically, the underlying mechanism of the coloration change in the mentioned 1D biological photonic structures can be understood according to the given formula

$$\lambda_{max} = 2(n_1 d_1 cos\theta_1 + n_2 d_2 cos\theta_2), \tag{3}$$

where d is the layer thickness, n is refraction index, and θ is angle of refraction. The subscripts represent the layer index. The angle of refraction at different layers θ_1 and θ_2 can be obtained from Snell's law $n_1 sin\theta_1 = n_1 sin\theta_1 = sin\theta_0$, where θ_0 is the incident angle from air. From the equation, it is easy to elucidate that either n, d, or θ_0 is related to the optical path in the multilayer and thus leads to shifting interference peaks at different wavelengths.

In biological system, high-dimensional photonic structures responsible for the coloration change are also discovered, though they are rare. An intriguing example is hercules beetles

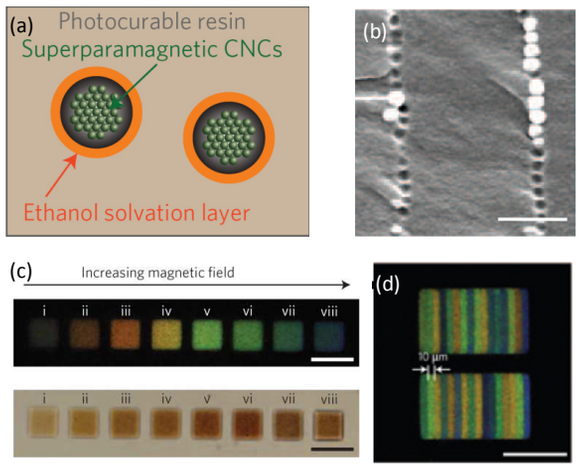

Figure 6. (Color online) Structural color printing using 'M-Ink' [57]. (a) Three-phase material system of 'M-Ink'; (b) 'M-Ink' particles align in a chain under external magnetic field, which acts as basic coloration units of color pattern after fixing by UV light; (c) Reflection images of multicolored structural colors (upper) and transmission photographs of the same sample (below) by gradually increasing magnetic fields; (d) High-resolution multiple structural color patterns. Scale bars: (b) 1μm, (c) and (d) 100 μm.

Dynastes hercules which can alter their appearance from khaki-green to black providing the ambience changes from dry to a high humidity level [54–56] (Fig. 5(g) and (h)). The 3D photonic crystal structures (nanoporous structures) are filled with water instead of air voids in dry status, rendering different refraction index contrast and thus the variation of Bragg scattering (Fig. 5(i), here only 2D cross section is illustrated). However, the underlying physics of coloration change induced by high-dimensional photonic structures is no other than that of their 1D counterparts.

2.2.2. Bio-inspired fabrications and applications

Due to the obvious appearance changes which are easy to be picked up with the naked eye, color-tunable devices are explored to identify the status changes by temperature, vapor, solvent, humidity in ambience, the applied mechanical force, electric field, magnetic field and etc. Besides the sensors, some novel writing system ('paper and ink') are developed. The key idea is to modify period (d), refraction index (n), viewangle (θ) or their combinations of photonic structures, just like nature shows us.

2.2.2.1. *d* variation

Because of relatively simple control by the environmental stimuli and large spectral variation which can be recognized by the naked eye, approaches on the modulation of photonic structure period are always of scientist interests in obtaining tunable color applications.

'M-Ink' is a mixture of colloidal nanocrystal clusters (CNCs), solvent and photocurable resin (Fig. 6(a)). With the superparamagnetic Fe_3O_4 nanocrystals encapsulated by silica shell, 'M-Ink' can response to external magnetic fields. The role of the resin is to provide repulsive force which balances the attractive force of the CNCs. Without external magnetic fields, CNCs are randomly dispersed (infinite period) in liquid resin. The exhibited coloration is consistent with the magnetite, to be brown. After applying magnetic fields, the CNCs are assembled to form chain-like structures along the magnetic field lines (Fig. 6(b)). The additional magnetic force, the intrinsic force among the CNCs, and the repulsive force by resin

establish dynamic balance with variation of the external magnetic fields, tuning the distance between the neighboring CNC (finite period). The switchable period then determines the color of the light diffracted from the CNC chain, leading to a full color show (Fig. 6(c)). The final step is to fix the desired coloration. After exposure to ultraviolet (UV) light at different exerted magnetic fields locations, the chain-like CNCs can be frozen in the solidified resin instantaneously, remaining the periods of the chains undistorted and accomplishing high-resolution color pattern fabrication (Fig. 6(d)) [57].

With similar principle, the electric field-driven tunable color sensor is also realized by highly charged polystyrene (PS) colloids which form non-close-packed face-centered cubic (fcc) lattice [58]. Tuning the period along [111] direction by the balance of the exerted electrostatic force and the repulsive force, the exhibited coloration changes as a result of the applied electric field. The so-called 'P-Ink' is an electroactive material which consists of inverse opal inside polyferrocenylsilane (PFS) derivatives matrix. Such ink fabrication includes 3 primary steps: An opal film made of silica spheres is deposited onto glass substrate first by self-assembly; UV light is exposed to the sample in order to solidify the matrix and then form a stable PFS/silica composite; With diluted HF, inverse opal structure are realized in the elastomeric polymer matrix. By applying tunable voltage, macroscopic swelling and shrinking of the polymer matrix and microscopic Bravais lattice change responsible for the reverse coloration occur [59]. Stimulated by electrical forces, quite a few switchable coloration devices or sensors based on other materials or circumstances can be found elsewhere [60–62].

Many pressure-based photonic and even laser devices are reported [63–66]. Using monodispersed PS spheres to form cubic close packing (ccp) structures which are embedded in polydimethylsiloxane (PDMS) matrix, reverse colors are observed simply by stretching and releasing the rubber sheet. Upon mechanical stress, the lattice is elongated along the applied force direction, while the interplanar spacing in the perpendicular direction (i.e. distance between the (111) planes) decreases because of the nearly invariance volume of the rubber. The compressed distance leads to a blue-shift, e.g., from red to green [63]. Such opal rubber is believed to have practical applications such as a color indicator, tension meter or elongation strain sensor. The inverse opal structures (filled by air voids) in elastomer network are also synthesized [64, 67] (Fig. 7(a)). The porous elastomeric photonic crystals (EPCs) show highly reversible optical response to compressive force, e.g., 60 nm spectral blue-shift under a compressive pressure of $\sim$ 15 kPa in the structures having 350-nm void size. Although the coloration change can be attributed to the Bravais lattice deformability, like the mechanism mentioned before. However, it is especially noteworthy that porous EPCs remain nearly undeformed in orthogonal directions when an external pressure is exerted in one direction, which can be ascribed to the high filling factor of air voids. The air voids enable the distortion of the cross-sectional void spaces from roughly circular to elliptical shape and a reduction of the air volume fraction under pressure. The elastic deformation feature of such structures helps to reduce the redistribution of stress along lateral directions when compressed by a patterned surface, leading to novel biometric applications such as the fingerprint recognition devices, as shown in Fig. 7(b). Additionally, air voids of porous EPCs provide a platform to incorporate with other functional materials for us to explore new applications. For instance, filling PbS quantum dots in the air voids, the photoluminescence (PL) emission, which leads to many potential applications in the near-infrared region, can be modified by overlapping with the forbidden bandgap of the inverse opal structures (Fig. 7(c)).

The chemical solvents are also used to be as stimuli. An interesting example is invention of new type 'photonic paper/ink' system [68, 69]. With novel soft materials consisting of

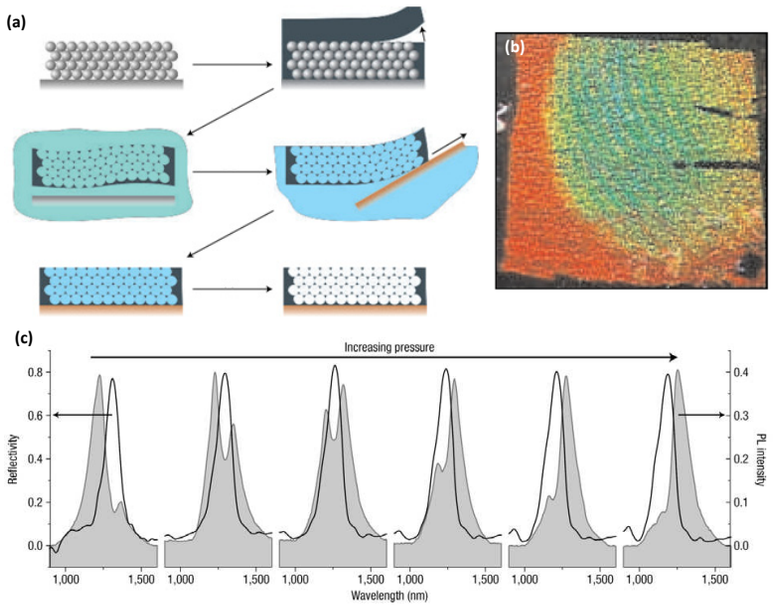

Figure 7. (Color online) From color fingerprinting to the control of photoluminescence in EPC films [67]. (a) Schematic diagram of the elastic inverse opal structure fabrication; (b) A captured still image of the EPC film under compression by an index finger; (c) NIR-emitting PL emission of colloidal PbS quantum dots which are incorporated into voids of the EPC can be tuned by overlapping the forbidden gap (solid black line) with the PL peak (grey filled curve).

closely packed PS and polymer elastomer (colloids and PDMS), the exhibited coloration can be altered reversely by immersing the materials into silicone liquid ('writing process') and an evaporation process ('erasing process'). The spacing between the (111) planes is adjusted by the strength of interaction between PDMS matrix and the contained silicone oligomers with different molecule weight in the liquid. With different solvents ('ink'), the swelling and shrinkage of the matrix show a featured reversible shift of Bragg diffraction peak. A multilayer based on alternating Teflon-like layer and Au nanoparticle/Teflon-like layer composite layer operates not in visible but optical telecommunication wavelength range [70]. When the structure is exposed to different organic solvent vapor (e.g. acetone, ethanol, methanol, water, chloroform, and etc.), the molecules enter the metal/polymer composite inside the holes and microvoids in its structure, resulting in the swelling up, e.g., for acetone vapors at a molar fraction of 0.25, with an relative increase of 12.5% in thickness to an equilibrium state while leaving the Teflon-like layer unchanged due to its inert chemical features. The measured reflectance show a large variation of 0.2 μm, which is advantageous to the detection of the organic/inorganic vapors.

Other external stimuli such as UV light, heat, or chemical reaction are applied to trigger and fabricate coloration sensitive materials as well by reversely controlling the spacing of the responsible photonic structures. Detailed information can be found in some references and recent reviews [14, 15, 61, 71–74].

2.2.2.2. *n* variation

Besides *d*, the refraction index *n* is another attribute of photonic structures. Different approaches to alter refraction index, in which infiltration is most regular, are revealed in order to achieve novel visual applications. Inspired by beetles *D. hercules*, 3D nanoporous structures are fabricated by so-called dip-coating deposition, achieving humidity sensing [75]. The 3D architecture, which is inverse opal structure, is reported to have its reflective peak

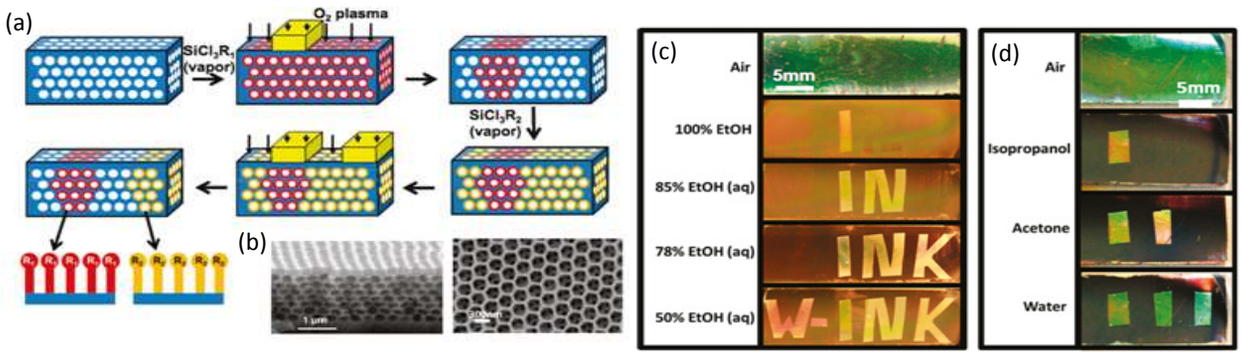

Figure 8. (Color online) Silica inverse opal films of 'Watermark-Ink' system [76]. (a) Schematic procedure of chemical encoding; (b) SEM images of the fabricated inverse opal structures in cross-sectional view (left) and top view (right); (c) Optical images of the fabricated film in which the word 'W-INK' is encoded via functional chemical groups on surfaces. (d) Optical images of different encoded patterns under different solvents.

red-shifting 14 nm when the relative humidity changes from 25% to 98%. It is worth noting that after treatments by O_2 plasma, the 3D photonic structures exhibit large bandgap shift of 137 nm and dramatic coloration change from bluish green in dry state to red in fully wet state. The modified hydrophilic feature play an important role in water collection in air voids at different level of humidity, leading to larger variation of refraction index contrast. The other clew for the remarkable coloration change can be ascribed to the high filling factor of air voids of inverse opal structures. The high value of $\sim$ 76% results in a wider modulation of refraction index contrast by the amount of solvent absorption. Tuning hydrophilic features by chemical groups, the inverse opal film can even be used as 'Watermark-Ink' system [76]. In the studies, the inside porous structures are functionalized with chemical group ($R1$, $R2$, $R3$, or $R4$) through vaporizing an alkylchlorosilane. The chemical functionalities of the structures then are erased and the surface is reactivated by O_2 plasma exposure, leaving a patterned functionalized region where is masked by a PDMS polymer. With iterations of such kind of functionalization and reactivation, the opal structures are locally patterned by different chemical groups, leading to differentiate hydrophilic feature (Fig. 8(a) and (b)). When immersing the film into specific fluids, regulated infiltration by the wettability occurs spatially in the film and thus surveys different optical responses (i.e. different patterns, Fig. 8(c) and (d)). The fabricated structures are expected to have applications in encryption as well as colorimeter.

Besides infiltration, phase-transition materials can also induce refraction index variation and switchable coloration, providing the transition conditions are satisfied. The best-known phase-transition material maybe is liquid crystals (LCs). Above the phase-transition temperature of 34°, LCs change their nematic phase which is anisotropic to isotropic phase, leading to a significant change of refraction index and coloration, e.g., in inverse opal structures. By mixing the active material into LCs, sensitive reflection and polarization triggered by UV light are reported by a series of subsequent researches [77–79]. Besides LCs, various sensitive materials, including Ag_2Se, WO_3 and ferroelectric ceramics, are also found functionally in incorporating with diversified photonic structures to obtain tunable structural coloration materials and thus fabricate thermo- or electro-sensors [80–83].

2.2.2.3. θ variation

Iridescence is a characteristic of structural coloration, which is determined by band dispersions of photonic structures. With various incident angle or observation direction, the

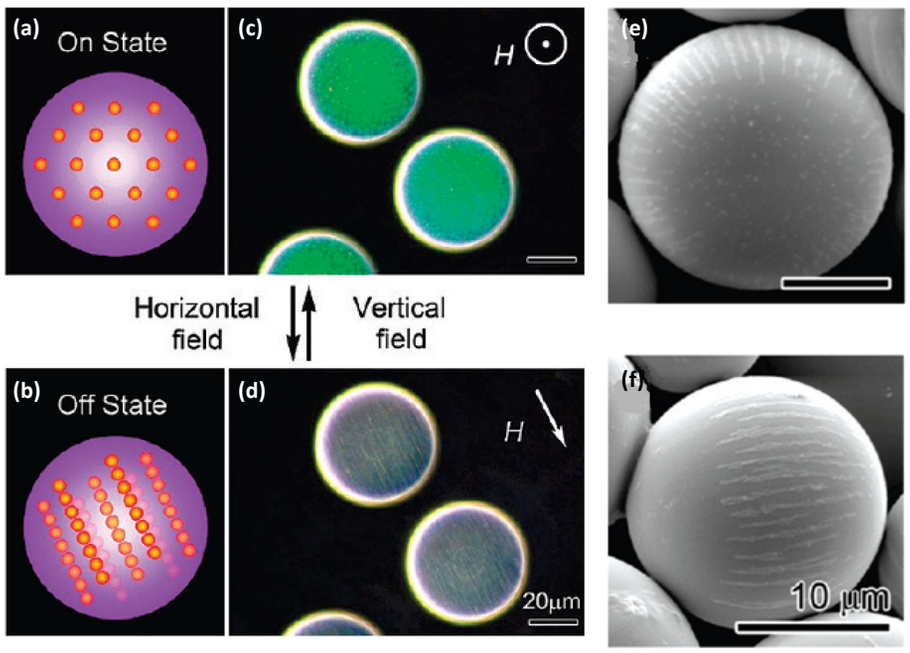

Figure 9. (Color online) Magnetochromatic microspheres switched between 'on' and 'off' states by rotating external fields [84, 85]. Schematic illustrations, optical images, and the corresponding SEM photographs of 'on' and 'off' states are (a), (c), (e), and (b), (d), (f), respectively.

perceived coloration is changing. Hence, it is feasible to explore novel tunable color devices by tuning orientations of the photonic structures [84–86]. Just like the fish neon tetra *P. innesi*, magnetochromatic microspheres alter their appearance by tilting the inner photonic structures with respect to the incidence (Fig. 9). As mentioned before, with superparamagnetic Fe_3O_4 particles coated by silica in PEGDA emulsions, the applied magnetic field guides to form photonic chains, in which the interpaticle distances depend on the balance of the attractive and repulsive force. Polymerized by UV light, microspheres are solidified and the inner periodic photonic chains, which give rise to structural coloration, are fixed permanently. Dispersing the microspheres into liquids, various colors are observed in top view due to the random orientations of the photonic chains in the microspheres. By applying external magnetic fields, the microspheres tend to rotate in order to keep the magnetic chains inside in the direction of the magnetic vector, leading to a homogenous coloration of green exhibited. The feature of the switchable coloration 'on' and 'off' status by the external stimuli is believed to have applications in color display, signage, bio- and chemical detection, and magnetic field sensing.

2.3. Structural color mixing and applications

2.3.1. Prototypes

Structural coloration results from the interaction of light and photonic structures with featured size of visible wavelengths. It is even more widespread than pigmentary coloration in animal world. Some literatures have well reviewed the field comprehensively. In the Chapter, we do not plan to pay attention to the overall structural coloration but only focus on a specific subject 'structural color mixing' [87–92]. In tiger beetles *Cicindela oregona*(Fig. 10(a)-(c)) [87, 88], the honeycomb-like pits are found on surfaces of the elytra. Under microscope, the brown morph actually includes blue-green patches in the red background, while the black one consists of magenta patterns surrounded by dull green. The microscopic colors are the results of

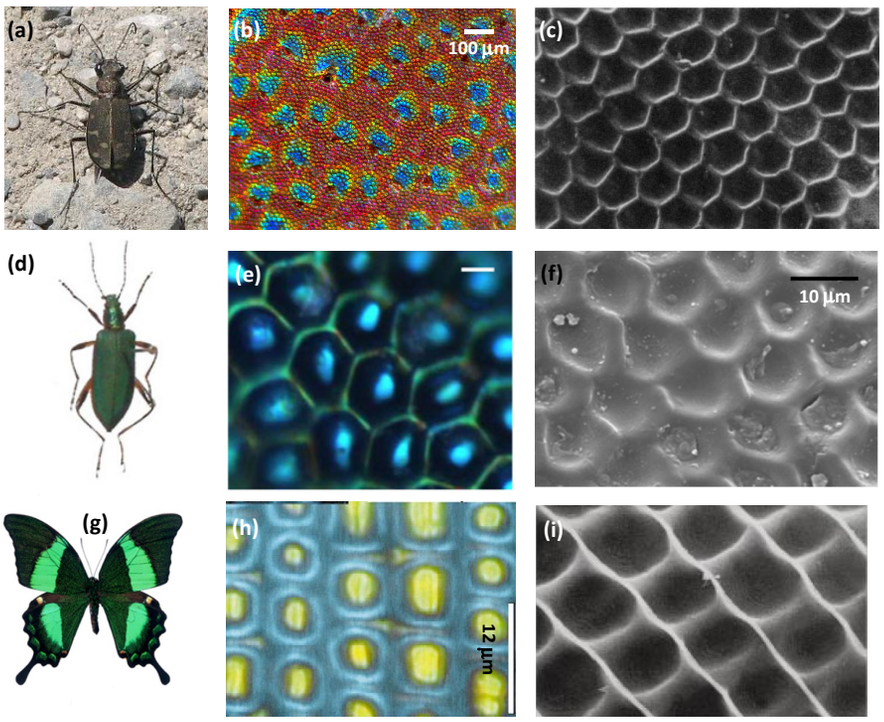

Figure 10. (Color online) Structural Color Mixing in Nature [87, 90, 91]. Photographs, optical microscopy and SEM images of tiger beetles *C. oregona* ((a), (b), (c)), long-jointed beetles *C. obscuripennis* ((d), (e), (f)), and swallowtail butterflies *P. palinurus* ((g), (h), (i)), respectively.

light interference by the multilayer structures in the cuticle. However, due to the colored patches (40-80 μm across) are too small to be resolved by the unaided eye (the resolution d is determined by the Rayleigh criterion $d{=}l\times 0.61\lambda/D$, where l is distance of distinct vision, λ the wavelength and D the average pupil diameter of humankind), the perceived coloration is a mixture of the discrete colors, leading to a totally different exhibition from that equipped with microscope. From the investigations of photonic structures of beetles *Chlorophila obscuripennis* (Fig. 10(d)-(f)), we revealed the color is a juxtaposition in a smaller region ($\sim 10\times 10$ μm^2) by green on the ridges and cyan in centers of the pits. Furthermore, the pits on the elytra surface give rise to diffused light reflected over a wide large of angles, leading to inconspicuous coloration shown [91]. In butterflies *Papilio palinurus* (Fig. 10(g)-(i)), the scanning electronic micrographs show surfaces in the scales comprise a similar two-dimensional (2D) pits (4-6 μm in diameter and 3 μm at the greatest depth). The flat regions between and in pits appear yellow, and the inclined region contributes to blue color. Because of the limitation of human eyes' resolution, the butterfly displays a mixture color of green, i.e. yellow plus blue turns to be green. Due to sufficient depth of the pits, light which normally incidents on the inclined side can experience dual reflection and is back-reflected. The retro-reflection is found to play a key role in the polarization conversion of incident light, which is crucial in some novel optical applications. Thanks to symmetric feature of the pits, no macroscopic polarization effects can be observed [90]. On the cover scale surfaces of butterflies *Suneve coronata*, however, the natural occurring triangular grooves array not symmetric but in 1D way with a period of ~ 2 μm, giving rise to polarization conversion of the normal incident light in a specific direction. Intriguingly, it is revealed the coloration macroscopically remains unconscious change under different polarized illumination. The reason is the curly scales, which induce polarization conversion between the neighboring rows of scales but in the

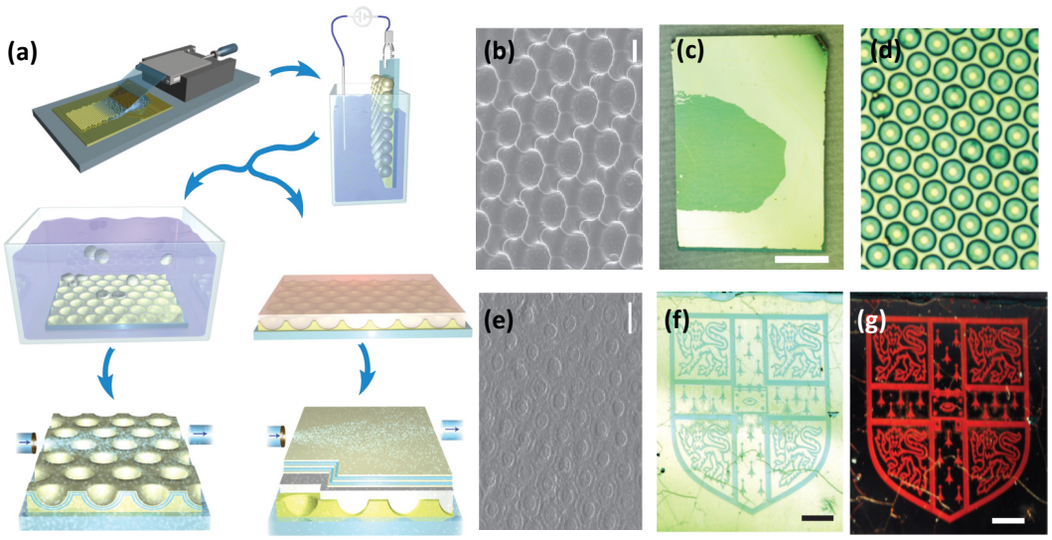

Figure 11. (Color online) Mixed structural coloration and applications inspired by nature [95]. (a) Schematic diagram of artificial samples mimicking the scale structures of *P. blumei*; (b) SEM photographs in top view show the concavities on surface of the replica which is (c) green macroscopically but (d) resolved yellow and green microscopically; (e) Modifications of the concavities morphology by melting colloidal spheres embedded in the concavities lead to a striking change in color of the sample from blue to red viewed (f) in direct specular reflection and (g) in retro-reflection. Scales: (a) 2 μm, (c)(f)(g) 5 mm, and (e) 5μm.

orthogonal direction. The nanostructures having different magnitude in size therefore cancel out the macroscopic polarization effects (Fig. 12(a)-(d)) [89].

2.3.2. Bio-inspired fabrications and applications

Structural coloration may be especially crucial for future color and related industry because of the non-fading feature (if the photonic structures are undeformed) [93, 94] and environmental friendliness. Naturally, structural coloration mixing inherits the advantages. Mimicking the nature, mixed structural color and its application can be obtained. For example, PS colloids with a diameter of 5 μm are assembled on a gold-coated silicon substrate. A 2.5-μm-thick layer of platinum or gold is then deposited to fill the interspaces of the colloids by electrochemical approach, creating a negative replica. After removal of the PS colloids by ultrasonic waves and a sputtering thin carbon film, a multilayer of quarter-wave titania and alumina films is grown by ALD (Fig. 11(a)), inheriting the morphology of hexagonally arranged pits of the negative replica (Fig. 11(b)). The sample exhibits similar color mixing with that of butterflies *P. blumei* (Fig. 11(c) and (d)). Moreover, by modifying the surface morphology of the imitation (Fig. 11(e)), even visual information, e.g., a picture, can be encoded into the photonic structures which display a striking appearance change from pale blue in the specular direction to red in retro-reflection (Fig. 11(f) and (g)). The bio-inspired work is expected to find applications in security labelling field or color industry such as painting and coating [95].

Inspired by color mixing researches, some novel applications based on polarization conversion are designed [89]. For instance, by etching periodic triangular-like grooves on surfaces of a flat multilayer, the film displays a coloration of green, which is actually a mixed color from yellow in the flat region and blue in the grooves in normal incidence, as shown in Fig. 12(e). Because of the broken symmetry of the 1D structures, the blue color can be suppressed by using a polarizer on light path, leading to the exhibited coloration change to

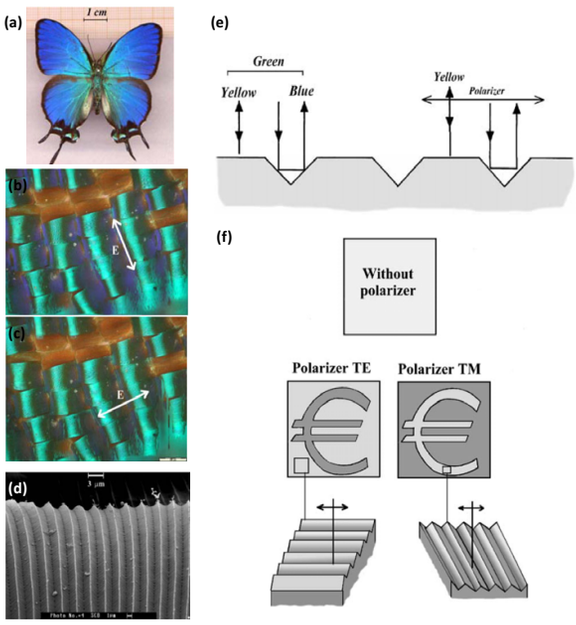

Figure 12. (Color online) (a) Optical image of a male *S. coronata* butterfly in dorsal view; The appearances under (b) TM and (c) TE polarization light show distinguished difference of the blue component, which can be attributed to (d) the broken symmetry of the triangular grooves in the surface plane; Two kinds of anti-fake or encryption designs, which apply (e) colored effect or (f) grey level change linked to the polarization and the broken surface symmetry, are inspired [89].

yellow (i.e. the hue in flat regions). That is, the grooved areas turn the light polarization $\pi/2$ and thus are shadowed by the inserted polarizer. Following the ideas, an encoded pattern which comprises grooved areas can be distinguished with the background consisting of perpendicular grooves via the luminosity level under different polarized light incidence (Fig. 12(f)). The two imaged examples inspired by the grooved structures of the butterfly show us great prospective in fields such as anti-fake and encryption.

2.4. Other bio-inspired fabrications and applications

Besides the main categories, some other bio-inspired photonic applications are also reported [96–100]. For examples, the natural scales of *Morpho sulkowskyi* are extremely sensitive to the different environmental vapors, which lead to dramatically improved responses as units of potential sensor applications compared with that of current devices[101]. Using black scales of the butterfly *Papilio paris* and *Thaumantis diores* as templates, hierarchically periodic microstructure titania replica was systhesized by chemical procedures. The high surface area inherited from the natural templates is great advantages to the light harvesting efficiency and dye sorption when the replica is used as photoanode in dye-sensitized solar cell [100]. With *Morpho* as bio-templates, alumina replicas show the potential applications in waveguides and beam-splitters under thin film coating by ALD and sintering [97]. Under thick film coating, the hybrid structure is found not to inherit the 'Christmas-tree' structures but develop a 'Pyramid-like' structures which have potential applications in light trapping [99]. With the complex photonic structures (multilayer plus 2D amorphous structures) of beetles *Trigonophorus rothschildi varians* as 'blueprints', the artificial counterpart which is fabricated by FIB etching holes through a $5\times$SiO/SiGe multilayer structure show similar optical features like non-specularity and only slightly angle-dependent reflectance [98]. Further bio-inspired work is undergoing which is stimulated by a recent revealed 3D architecture [102], aiming

at the ultra-negative angular dispersion of diffraction and potential novel dispersive optical elements.

3. Perspectives

In the Chapter, several important kinds of bio-inspired photonic applications are reviewed, including antireflection devices, color-tunable sensors, structural color mixing applications and etc. The nature nourishes scientists the functional optical applications either the blueprints of photonic architecture or directly the bio-templates. Due to the higher index of inorganic materials used, the mimicking photonic structures even show better optical performances as well as enhanced mechanical properties of high temperature tolerance, stability and infrangibility. The biomimetic applications are anticipated to help our life better in the near future. However, complicated photonic structures (e.g. those of high-dimensional, hierarchic, amorphous features in nature) still remains hardly reproduced or, if they are fabricated successfully, the efforts involved are so great using the traditional fabrication ways that optical devices can not commercially explored. Thorough physical mechanism understanding as well as better fabrication approach explorations may help to simply the structure fabrications, achieve similar optical functions and realize commercial applications. In addition, adding substances such as functional chemical groups, fluorescence particles, metal, or other active materials, the mimicking photonic structures allow the properties of interest to be augmented, which may open a new window of novel optical device exploration. Although the photonic biomimicry is in its infancy, we believe that the bio-inspired optical device would surely have profound impacts on our modern society.

Author details

Feng Liu
Laboratory of Opto-electrical Material and Device, Department of Physics, Shanghai Normal University, Shanghai, China

Biqin Dong
Department of Mechanical Engineering, Northwestern University, Evanston, USA

Xiaohan Liu
Department of Physics, Fudan University, Shanghai, China

4. References

[1] Yablonovitch, E. (1987). Inhibited Spontaneous Emission in Solid-State Physics and Electronics. *Phys. Rev. Lett.*, Vol.58: 2059–2062.
[2] John, S. (1987). Strong localization of photons in certain disordered dielectric superlattices. *Phys. Rev. Lett.*, Vol.58: 2486–2489.
[3] Joannopoulos, J.D.; Johnson, S.G.; Winn J.N.; & Meade, R.D. (2008). *Photonic Crystals: Molding the Flow of Light*, 2nd Ed. Princeton University Press, Princeton and Oxford, USA.
[4] Fox, D.L. (1976). *Animal Biochromes and Structural Colours*, University of California Press, Berkeley, USA.
[5] Srinivasarao, M. (1999). Nano-Optics in the biological world: beetles, butterflies, birds, and moths. *Chem. Rev.*, Vol.99: 1935–1961.

[6] Vukusic, P. & Sambles, J.R. (2003). Photonic structures in biology. *Nature*, Vol.424: 852–855.
[7] Parker, A.R. (2005). A geological history of reflecting optics. *J. R. Soc. Interface*, Vol.2: 1–17.
[8] Seago, A. Brady, P. Vigneron, J-P. & Schultz, T.D. (2009). Gold bugs and beyond: a review of iridescence and structural colour mechanisms in beetles (Coleoptera). *J. R. Soc. Interface*, Vol.6: S165–S184.
[9] Shawkey, M.D. Morehouse, N.I. & Vukusic, P. (2009). A protean palette: colour materials and mixing in birds and butterflies. *J. R. Soc. Interface*, Vol.6: S221–S231.
[10] Kinoshita, S. & Yoshioka, S. (2005). Structural colors in nature: the role of regularity and irregularity in the structure. *ChemPhysChem*, Vol.6: 1442–1459.
[11] Parker, A.R. & Townley, H.E. (2007). Biomimetics of photonic nanostructures. *Nat. Nanotech.*, Vol.2: 347–353.
[12] Pulsifer, D.P. Lakhtakia, A. (2011). Background and survey of bioreplication techniques. *Bioinsp. Biomim.*, Vol.6(No. 031001).
[13] Chung, W-J. Oh, J-W. Kwak, K. Lee, B.Y. Meyer, J. Wang, E. Hexemer, A. & Lee, S-W. (2011). Biomimetic self-templating supramolecular structures. *Nature*, Vol.478: 364–368.
[14] Fudouzi, S. (2011). Tunable structural color in organisms and photonic materials for design of bioinspired materials. *Sci. Technol. Adv. Mater.*, Vol.12(No.064704).
[15] Zhao, Y. Xie, Z. Gu, H. Zhu, C. & Gu, Z. (2012). Bio-inspired variable structural color materials. *Chem. Soc. Rev.*, Vol.41: 3297–3317.
[16] (b) Li, Y. Zhang, J. & Yang, B. (2010). Antireflective surfaces based on biomimetic nanopillared arrays. *Nano Today*, Vol.5: 117–127.
[17] Land, M.F.; & Nilsson, D.E. (2001). *Animal Eyes.*, Oxford University Press, Oxford, UK.
[18] Yoshida, A. Motoyama, M. Kosaku, A. & Miyamoto, K. (1997). Antireflective nanoproturberance array in the transparent wing of a hawkmoth Cephanodes hylas. *Zool. Sci.*, Vol.14: 737–741.
[19] Zhang, G. Zhang, J. Xie, G. Liu, Z. & Shao, H. (2006). Cicada wings: a stamp from nature for nanoimprint lithography. *Small*, Vol.2(No.12): 1440–1443.
[20] Born, M. Wolf, E. (1999). *Principles of Optics*, 7th Ed. Cambridge University Press, Cambridge, UK.
[21] Xi, J.-Q. Schubert, M.F. Kim, J.H. Schubert, E.F. Chen, M. Lin, S. Liu, W. & Smart, J.A. (2007). Optical thin-film materials with low refractive index for broadband elimination of Fresnel reflection. *Nat. Photon.*, Vol.1: 176–179.
[22] Martín-Palma, R.J. Pantano, C.G. & Lakhtakia, A. (2008). Replication of fly eyes by the conformal-evaporated-film-by-rotation technique. *Nanotechnology*, Vol.19 (No.355704).
[23] Yang, S-M. (2006). Nanomachining by colloidal lithography. *Small*, Vol.2(No.4): 458–475.
[24] Pearton, S.J. & Norton, D.P. (2005). Dry etching of electronic oxides, polymers, and semiconductors. *Plasma Process. Polym.*, Vol.2: 16–37.
[25] Hsu, C. Lo, H. Chen, C. Wu, C.T. Hwang, J. Das D. Tsai, J. Chen, L. & Chen K. (2004). Generally applicable self-masked dry etching technique for nanotip arrayfabrication. *Nano Lett.*, Vol.4 (No.3): 471–475.
[26] Hsu, C. Huang, Y.F. Chen L.C. Chattopadhyay, S. Chen, K.H. Lo, H.C. & Chen, C.F. (2006). Morphology control of silicon nanotips fabricated by electron cyclotron resonanceplasma etching. *J. Vac. Sci. Technol. B*, Vol.24(No.1): 308–311.
[27] Huang, Y. Huang, Chattopadhyay, S. Jen, Y. Peng, C. Liu, T. Hsu, Y. Pan, C. Lo. H. Hsu, C. Chang Y. Lee, C. Chen, K. & Chen L. (2007). Improved broadband and quasi-omnidirectional anti-reflection properties with biomimetic silicon nanostructures. *Nat. Nanotech.*, Vol.2: 770–774.

[28] Gao, H. Liu, Z. Zhang, J. Zhang, G. & Xie, G. (2007). Precise replication of antireflective nanostructures from biotemplates. *Appl. Phys. Lett.*, Vol.90(No. 12): 1–3.
[29] Huang, J. Wang, X. & Wang, Z.L. (2008). Bio-inspired fabrication of antireflection nanostructures by replicating fly eyes. *Nanotechnology*, Vol.19(No.025602).
[30] Green, M.A. (1987). *Higher Efficiency Silicon Solar Cells*, Trans Tech Pub, Aedermannsdorf, Switzerland.
[31] Zhao, J. & Green, M.A. (1991). Optimized antireflection coatings for high-efficiency silicon solar cells. *IEEE Trans. Electron Devices*, Vol.38(No.8): 1925–1934.
[32] Zhu, J. Hsu, C. Yu, Z. Fan, S. & Cui, Y. (2010). Nanodome Solar Cells with Efficient Light Management and Self-Cleaning. *Nano Lett.*, Vol.6(No.6): 1979–1984.
[33] Chen, H.L. Chuang, S.Y. Lin, C.H. & Lin, Y.H. (2007). Using colloidal lithography to fabricate and optimize sub-wavelength pyramidal and honeycomb structures in solar cells. *Opt. Express*, Vol.15: 14793–14803.
[34] Wang, K.X. Yu, Z. Liu, V. Cui, Y. & Fan S. (2012). Absorption enhancement in ultrathin crystalline silicon solar cells with antireflection and light-trapping nanocone gratings. *Nano Lett.*, Vol.12(No.3): 1616–1619.
[35] Ishimori, M. Kanamori, Y. Sasaki, M. Hane, K. & Xie, G. (2002). Subwavelength antireflection gratings for light emitting diodes and photodiodes fabricated by fast atom beam etching. *Jpn. J. Appl. Phys.*, Vol.41: 4346–4349.
[36] (a) Li, Y. Li, F. Zhang, J. Wang, C. Zhu, S. Yu, H. Wang, Z. & Yang, B. (2010). Improved light extraction efficiency of white organic light-emitting devices by biomimetic antireflective surfaces. *Appl. Phys. Lett.*, Vol. 96(No.153305).
[37] Song, Y.M. Choi, E.S. Park, G.C. Park, C.Y. Jang, S.J. & Lee Y.T. (2010). Disordered antireflective nanostructures on GaN-based light-emitting diodes using Ag nanoparticles for improved light extraction efficiency. *Appl. Phys. Lett.*, Vol.97(No. 093110).
[38] Lee, C. Bae, S.Y. Mobasser, S. & Manohara, H. (2005). A novel silicon nanotips antireflection surface for the micro Sun sensor. *Nano Lett.*, Vol.5(No.12): 2438–2442.
[39] Cong, H. Yu, B. & Zhao, X.S. (2011). Imitation of variable structural color in *paracheirodon innesi* using colloidal crystal films. *Opt. Express*, Vol.19(No.13): 12799–12808.
[40] Hadley, N.F. (1979). Wax secretion and color phases of the desert Tenebrionid beetle *Cryptoglossa verrucosa* (LeConte). *Science*, Vol.203: 367–369.
[41] Mäthger, L.M. Land, M.F. Siebeck, U.E. & Marshall, N.J. (2003). Rapid colour changes in multilayer reflecting stripes in the paradise whiptail, *Pentapodus paradiseus*. *J. Exp. Biol.*, Vol.206: 3607–3613.
[42] McClain, E. Seely, M.K. Hadley, N.F. & Fray, V. (1985). Wax blooms in Tenebrionid beetles of the Namib desert: correlations with environment. *Ecology*, Vol.66: 112–118.
[43] Jolivet, P. (1994). Phsiological colour changes in tortoise beetles, In: *Novel Aspect of the Biology of Chrysomelidae*, Cox, M.L. & Petitpierre, E., (Eds.), page numbers (331-335), Kluwer Academic, Netherland.
[44] Vigneron, J.P. Pasteels, J.M. Windsor, D.M. Vertésy, Z. Rassart, M. Seldrum, T. Dumont, J. Deparis, O. Lousse, V. Biró, L.P. Ertz, D. & Welch, V. (2007). Switchable reflector in the Panamanian tortoise beetle *Charidotella egregia* (Chrysomelidae: Cassidinae). *Phys. Rev. E.*, Vol.76(No. 031907).
[45] Mason, C.W. (1929). Transient color changes in the tortoise beetles (Coleoptera: Chrysomelidae). *Entomol. News*, Vol.45: 52–56.
[46] Eliason, C.M. & Shawkey, M.D. (2010). Rapid, reversible response of iridescent feather color to ambient humidity. *Opt. Express*, Vol.18(No.20): 21284–21292.

[47] Kasukawa, H. Oshima, N. & Fujii, R. (1986). Control of chromatophore movements in dermal chromatic units of blue damselfish-II. The motile iridophore. *Comp. Biochem. Physiol. C*, Vol.83: 1–7.
[48] Kasukawa, H. Oshima, N. & Fujii, R. (1987). Mechanism of light reflection in blue damselfish motile iridophore. *Zool. Sci.*, Vol.4: 243–257.
[49] Oshima, N. & Fujii, R. (1987). Mobile mechanisms of blue damselfish (*Chrysiptera cyanea*) iridophores *Cell Motil. Cytoskel.*, Vol.8: 85–90.
[50] Liu, F. Bong, B.Q. Liu, X.H. Zheng, Y.M. & Zi, J. (2009). Structural color change in longhorn beetles *Tmesisternus isabellae*. *Opt. Express*, Vol.17(No.18): 16183–16191.
[51] Lythgoe, J.N. & Shand, J. (1982). Changes in spectral reflexions from the iridophores of the neon tetra. *J. Physiol.*, Vol.325: 23–34.
[52] Oshima, N. (2005). Light reflection in motile iridophores of Fish, In: *Structural Colors in Biological SystemsąłPrinciples and Applications*, Kinoshita, S. & Yoshioka, S., (Eds.), page numbers (211), Osaka University Press, Japan.
[53] Yoshioka, S. Matsuhana, B. Tanaka, S. Inouye, Y. Oshima, N. & Kinoshita, S. (2011). Mechanism of variable structural colour in the neon tetra: quantitative evaluation of the Venetian blind model. *J. R. Soc. Interface*, Vol.8: 56–66.
[54] Hinton, H.E. & Jarman, G.M. (1972). Physiological colour change in the Hercules beetle. *Nature*, Vol.238: 160–161.
[55] Hinton, H.E. & Jarman, G.M. (1973). Physiological colour changes in the elytra of the Hercules beetles, Dynastes hercules. *J. Insect Physiol.*, Vol.19: 533–549.
[56] Rassart, M. Colomer, J-F. Tabarrant, T. Vigneron, J.P. (2008). Diffractive hygrochromic effect in the cuticle of the hercules beetle *Dynastes hercules*. *New J. Phys.*, Vol.10(No. 033014).
[57] Kim, H. Ge, J. Kim, J. Choi, S. Lee, H. Lee, H. Park, W. Yin, Y. & Kwon, S. (2009). Structural colour printing using a magnetically tunable and lithographically fixable photonic crystal. *Nat. photon.*, Vol.3: 534–540.
[58] Shim, T.S. Kim, S-H. Sim, J.Y. Lim, J-M. & Yang, S-M. (2010). Dynamic Modulation of Photonic Bandgaps in Crystalline Colloidal Arrays Under Electric Field. *Adv. Mater.*, Vol.22: 4494–4498.
[59] Puzzo, D.P. Arsenault, A.C. Manners, I. & Ozin, G.A. (2009). Electroactive Inverse Opal: A Single Material for All Colors. *Angew. Chem., Int. Ed.*, Vol.47: 943–347.
[60] Arsenault, A.C. Puzzo, D.P. Manners, I. & Ozin, G.A. (2007). Photonic-crystal full-colour displays. *Nat. Photon.*, Vol.1: 468–472.
[61] Walish, J.J. Kang, Y. Mickiewicz, A. & Thomas E.L. (2009). Bioinspired electrochemically tunable block copolymer full color pixels. *Adv. Mater.*, Vol.21: 3078–3081.
[62] Hwang, K. Kwak, D. Kang, C. Kim, D. Ahn Y. & Kang, Y. (2011). Electrically tunable hysteretic photonic gels for nonvolatile display pixels. *Angew. Chem., Int. Ed.*, Vol.50: 6311–6314.
[63] Fudouzi, H. & Sawada, T. (2006). Photonic rubber sheets with tunable color by elastic defornmation. *Langmuir*, Vol.22(No.3): 1365–1368.
[64] Sumioka, K. Kayashima, H. & Tsutsui, T. (2002). Tuning the Optical Properties of Inverse Opal Photonic Crystals by Deformation. *Adv. Mater.*, Vol.13(No.18): 1284–1286.
[65] Fudouzi, S. Kanai, T. & Sawada, T. (2011). Widely tunable lasing in a colloidal crystal gel film permanently stabilized by an ionic liquid. *Adv. Mater.*, Vol.23(No.33): 3815–3820.
[66] Arsenault, A.C. Kitaev, V. Manners, I. Ozin, G.A. Mihi, A. & Míguez, H. (2005). Vapor swellable colloidal photonic crystals with pressure tunability. *J. Mater. Chem.*, Vol.15: 133–138.

[67] Arsenault, A.C. Clark, T.J. Freymann, G.V. Cademartiri, L. Sapienza, R. Bertolotti, J. Vekris, E. Wong, S. Kitaev, V. Manners, I. Wang, R.Z. John, S. Wiersma, D. & Ozin, G.A. (2006). From colour fingerprinting to the control of photoluminescence in elastic photonic crystals. *Nat. Mater.*, Vol.5: 179–184.
[68] (a) Fudouzi, H. & Xia, Y. (2003). Photonic papers and inks: color writing with colorless materials. *Adv. Mater.*, Vol.15(No.11): 892–896.
[69] (b) Fudouzi, H. & Xia, Y. (2003). Colloidal crystals with tunable colors and their use as photonic papers. *Langmuir*, Vol.19(No.23): 9653–9660.
[70] Convertino, A. Capobianchi, A. Valentini, A. & Emilio, N.M.C. (2003). A new approach to organic solvent detection: high-reflectivity Bragg reflectors based on a gold nanoparticle/Teflon-like composite material. *Adv. Mater.*, Vol.15(No.13): 1103–1105.
[71] Weissman, J.M. Sunkara, H.B. Tse, A.S. & Asher, S.A. (1996). Thermally Switchable Periodicities and Diffraction from Mesoscopically Ordered Materials. *Science*, Vol.274(No.5289): 959–963.
[72] Holtz, J.H & Asher, S.A. (1997). Polymerized colloidal crystal hydrogel films as intelligent chemical sensing materials. *Nature*, Vol.389: 829–832 .
[73] Hu, Z. Lu, X. & Gao, J. (2001). Hydrogel opals. *Adv. Mater.*, Vol.13(No.22): 1708–1712.
[74] Gates, B. Park, S.H. & Xia, Y. (2000). Tuning the photonic bandgap properties of crystalline arrays of polystyrene beads by annealing at elevated temperatures. *Adv. Mater.*, Vol.12(No. 9): 653–655.
[75] Kim, J.H. Moon, J.H. Lee, S-Y. & Park, J. (2010). Biologically inspired humidity sensor based on three-dimensional photonic crystals. *Appl. Phys. Lett.*,Vol.97(No.103701).
[76] Burgess, I.B. Mishchenko, L. Hatton, B.D. Kolle, M. Loncar M. & Aizenberg, J.(2011). Encoding complex wettability patterns in chemically functionalized 3D photonic crystals. *J. Am. Chem. Soc.*, Vol.133: 12430–12432.
[77] Kubo, S. Gu, Z.Z. Takahashi, K. Ohko, Y. Sato, O. & Fujishima, A. (2002). Control of the optical band structure of liquid crystal infiltrated inverse opal by a photoinduced nematic-isotropic phase transition. *J. Am. Chem. Soc.*, Vol.124: 10950–10951.
[78] Kubo, S. Gu, Z.Z. Takahashi, K. Fujishima, A. Segawa, H. & Sato, O. (2004). Tunable photonic band Gap crystals based on a liquid crystal-infiltrated inverse opal structure. *J. Am. Chem. Soc.*, Vol.126: 8314–8319.
[79] Kubo, S. Gu, Z.Z. Takahashi, K. Fujishima, A. Segawa, H. & Sato, O. (2005). Control of the optical properties of liquid crystal-infiltrated inverse opal structures using photo irradiation and/or an electric field. *Chem. Mater.*, Vol.17: 2298–2309.
[80] Jeong, U. & Xia, Y.N. (2005). Photonic crystals with thermally switchable stop bands fabricated from Se@Ag_2Se spherical colloids. *Angew. Chem., Int. Ed.*, Vol.44: 3099–3103.
[81] Li, B. Zhou, J. Li, L. Wang, J. Liu, X.H. & Zi, J. (2003). Ferroelectric inverse opals with electrically tunable photonic band gap . *Appl. Phys. Lett.*, Vol.83: 4704–4706.
[82] Kuai, S-L. Bader, G. & Ashrit, P.V. (2005). Tunable electrochromic photonic crystals. *Appl. Phys. Lett.*, Vol.86(No.221110).
[83] Khalack, J. & Ashrit, P.V. (2006). Tunable pseudogaps in electrochromic WO_3 inverted opal photonic crystals. *Appl. Phys. Lett.*, Vol.89(No.211112).
[84] Kim, S. Jeon, S. Jeong, W.C. Pank, H.S. & Yang, S. (2008). Optofluidic Synthesis of Electroresponsive Photonic Janus Balls with Isotropic Structural Colors. *Adv. Mater.*, Vol.20(No.21): 4129–4134.
[85] Ge, J. Lee, H. He, L. Kim, J. Lu, Z. Kim, H. Goebl, J. Kwon, S. & Yin, Y. (2009). Magnetochromatic microspheres: rotating photonic crystals. *J. Am. Chem. Soc.*, Vol.131(No.43): 15687–15694.

[86] Kim, J. Song, Y. He, L. Kim, H. Lee, H. Park, W. Yin, Y. & Kwon, S. (2011). Real-time optofluidic synthesis of magnetochromatic microspheres for reversible structural color patterning. *Small*, Vol.7: 1163–1168.
[87] Schultz, T.D. & Rankin, M.A. (1985). The ultrastructure of the epicuticular interference reflectors of tiger beetles(Cicindela). *J. Exp. Biol.*, Vol.117: 87–110.
[88] Schultz, T.D. & Rankin, M.A. (1989).Schultz, T.D. & Bernard, G.D. (1989). Pointillistic mixing of interference colours in cryptic tiger beetles. *Nature*, Vol.337: 72–73.
[89] Berthier, J. Boulenguez, J. & Balint, Z. (2007). Multiscaled polarization effects in *Suneve coronata* (Lepidoptera) and other insects: application to anti-counterfeiting of banknotes. *Appl. Phys. A*, Vol.86(No.1): 123–130.
[90] Vukusic, P. Sambles, J.R. & Lawrence, C.R. (2000). Colour mixing in wing scales of a butterfly. *Nature*, Vol.404: 457.
[91] Liu, F. Yin, H.W. Dong, B.Q. Qing, Y.H. Zhao, L. Meyer, S. Liu, X.H. Zi, J. & Chen, B. (2008). Inconspicuous structural coloration in the elytra of beetles *Chlorophila obscuripennis* (Coleoptera). *Phys. Rev. E*, Vol.77(No.012901).
[92] Liu, F. Wang, G. Jiang, L.P. & Dong, B.Q. (2010). Structural colouration and optical effects in the wings of *Papilio peranthus*. *J. Opt.*, Vol.12(No.065301).
[93] Vinther, J. Briggs, D.E.G. Clarke, J. Mayr, G. & Prum, R.O. (2010). Structural coloration in a fossil feather. *Biol. Lett.*, Vol.6: 128–131.
[94] Parker, A.R. (2000). 515 million years of structural colour. *J. Opt. A: Pure Appl. Opt.*, Vol.2: R15–R28.
[95] Kolle, M. Salgard-Cunha, P.M. Scherer, M. Huang, F.M. Vukusic, P. Mahajan, S. Baumberg, J.J. & Steiner, U. (2010).Mimicking the colourful wing scale structure of the Papilio blumei butterfly. *Nat. Nanotechnol.*, Vol.5: 511–515.
[96] Vukusic, P., Kelly R. & Hooper I. (2009). A biological sub-micron thickness optical broadband reflector characterized using both light and microwaves. *J. R. Soc. Interface*, Vol.6: S193–S201.
[97] Huang, J. Wang, X. & Wang, Z.L. (2008). Controlled replicaton of butterfly wings for achieving tunable photonic properties. *Nano Lett.*, Vol.6(No.10): 2325–2331.
[98] Biro, L.P. Kertesz, K. Horvath, E. Mark, G.I. Molnar, G. Vertesy, Z. Tsai, J.-F. Kun, A. Bailint,Z. & Vigneron, J.P.(2009). Bioinspired artificial photonic nanoarchitecture using the elytron of the beetle Trigonophorus rothschildi varians as a 'blueprint'. *J. R. Soc. Interface*, Vol.7(No.47): 887–894.
[99] Liu, F. Shi, W.Z. Hu, X.H. & Dong, B.Q. (2012). Hybrid structures and the optical effects in *Morpho* scales with thin and thick coatings using an atomic layer deposition method. Unpublished data.
[100] Zhang, W. Zhang, D. Fan, T.X. Gu, J.J, Ding, J. Wang, H. Guo, Q. & Ogawa, H. (2009). Novel Photoanode Srucure Templated from Butterfly Wing Scales. *Chem. Mater.*, Vol.21(No.1): 33–40.
[101] Potyrailo, R.A. Ghiradella, H. Vertiatchikh, A. Dovidenko, K. Cournoyer, J.R. & Olson, E. (2007). Morpho butterfly wing scales demonstrate highly selective vapour response. *Nat. photon.*, Vol.1: 123–128.
[102] Liu, F. Dong, B.Q. Zhao, F, Hu, X. Liu, X. Zi, J. (2011). Ultranegative angular dispersion of diffraction in quasiordered biophotonic structures *Opt. Express*, Vol.19(No.8): 7750–7755.